

REPORT DOCUMENTATION PAGE			Form Approved OMB No. 0704-0188	
<small>Public reporting burden for this collection of information is estimated to average 1 hour per response, including the time for reviewing instructions, searching existing data sources, gathering and maintaining the data needed, and completing and reviewing this collection of information. Send comments regarding this burden estimate or any other aspect of this collection of information, including suggestions for reducing this burden to Department of Defense, Washington Headquarters Services, Directorate for Information Operations and Reports (0704-0188), 1215 Jefferson Davis Highway, Suite 1204, Arlington, VA 22202-4302. Respondents should be aware that notwithstanding any other provision of law, no person shall be subject to any penalty for failing to comply with a collection of information if it does not display a currently valid OMB control number. PLEASE DO NOT RETURN YOUR FORM TO THE ABOVE ADDRESS.</small>				
1. REPORT DATE (DD-MM-YYYY) 01-08-2004		2. REPORT TYPE		3. DATES COVERED (From - To)
4. TITLE AND SUBTITLE Strength Degradation of Filament-Wound Graphite/Epoxy Tubes Due to Either Impact Damage or Fabrication Defects		5a. CONTRACT NUMBER F04701-00-C-0009		
		5b. GRANT NUMBER		
		5c. PROGRAM ELEMENT NUMBER		
6. AUTHOR(S) D. J. Chang and H. A. Katzman		5d. PROJECT NUMBER		
		5e. TASK NUMBER		
		5f. WORK UNIT NUMBER		
7. PERFORMING ORGANIZATION NAME(S) AND ADDRESS(ES) The Aerospace Corporation Laboratory Operations El Segundo, CA 90245-4691		8. PERFORMING ORGANIZATION REPORT NUMBER TR-2003(1413)-1		
9. SPONSORING / MONITORING AGENCY NAME(S) AND ADDRESS(ES) Space and Missile Systems Center Air Force Space Command 2450 E. El Segundo Blvd. Los Angeles Air Force Base, CA 90245		10. SPONSOR/MONITOR'S ACRONYM(S) SMC		
		11. SPONSOR/MONITOR'S REPORT NUMBER(S) SMC-TR-04-19		
12. DISTRIBUTION/AVAILABILITY STATEMENT Approved for public release; distribution unlimited.				
13. SUPPLEMENTARY NOTES				
14. ABSTRACT Two test series were conducted to assess the strength degradation of filament-wound graphite/epoxy tubes caused by impact damage or fabrication defects. The defects were either helical wrinkles or a hoop wrinkle inside the tube walls. The baseline tube configuration had a nine-ply (+10°, -10°, 90°) ₃ lay-up, with the exception of one tube having a (+15°, -15°, 90°, 90°) ₃ stacking sequence. The latter lay-up configuration was to induce helical fiber-dominated failure. The tubes were subjected to either pneumatic or hydrostatic internal pressure, creating a biaxial stress state in the tube walls. The test results show that the burst pressure decreases significantly with increasing impact force for impact-damaged tubes. For impact loads of 823 to 1470 N (185 to 330 lb), the burst pressure dropped by 24% to 32%, respectively, compared to those with no impact damage. Most failures initiated at the impact locations. Some originated from locations other than the impact sites. For the wrinkle-defect specimens, minor helical wrinkles had no measurable effect on the burst pressure. More severe helical wrinkles decreased the burst pressure by 8%. Hoop wrinkles caused a significant degradation in strength (14% on average).				
15. SUBJECT TERMS Filament-wound graphite epoxy tubes, Impact damage, Fiber wrinkles, Strength degradation				
16. SECURITY CLASSIFICATION OF:			17. LIMITATION OF ABSTRACT	18. NUMBER OF PAGES 13
a. REPORT UNCLASSIFIED	b. ABSTRACT UNCLASSIFIED	c. THIS PAGE UNCLASSIFIED		
				19a. NAME OF RESPONSIBLE PERSON Dick Chang
				19b. TELEPHONE NUMBER (include area code) (310)336-5808

20041008 445

Strength Degradation of Filament-Wound Graphite/Epoxy Tubes Due to Either Impact Damage or Fabrication Defects

1 August 2004

Prepared by

D. J. CHANG and H. A. KATZMAN
Space Materials Laboratory
Laboratory Operations

Prepared for

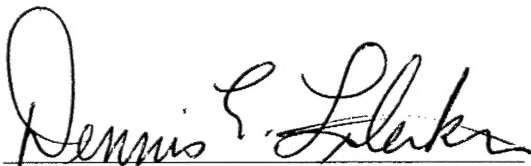
SPACE AND MISSILE SYSTEMS CENTER
AIR FORCE SPACE COMMAND
2430 E. El Segundo Boulevard
Los Angeles Air Force Base, CA 90245

Space Systems Group

This report was submitted by The Aerospace Corporation, El Segundo, CA 90245-4691, under Contract No. F04701-00-C-0009 with the Space and Missile Systems Center, 2430 E. El Segundo Blvd., Los Angeles Air Force Base, CA 90245. It was reviewed and approved for The Aerospace Corporation by P. D. Fleischauer, Principal Director, Space Materials Laboratory. LtCol Dennis Lileikis was the project officer for the program.

This report has been reviewed by the Public Affairs Office (PAS) and is releasable to the National Technical Information Service (NTIS). At NTIS, it will be available to the general public, including foreign nationals.

This technical report has been reviewed and is approved for publication. Publication of this report does not constitute Air Force approval of the report's findings or conclusions. It is published only for the exchange and stimulation of ideas.

A handwritten signature in black ink, appearing to read "Dennis Lileikis", written over a horizontal line.

LtCol Dennis Lileikis
SMC/CLT

Contents

1.	Introduction.....	1
2.	Test Series.....	3
2.1	Tubes with Impact Damage	3
2.2	Tubes with Fabricated Defects.....	3
3.	Test Results.....	5
3.1	Tubes with Impact Damage	5
3.2	Tubes with Fabricated Defects.....	6
3.2.1	Tubes Without Wrinkles.....	6
3.2.2	Tubes with minor helical defects.....	7
3.2.3	Tubes with hoop defects	8
3.2.4	Tubes with severe helical defects.....	8
4.	Summary	11
	References	13

Figures

1.	Outside view of tube specimen with end fittings.	1
2.	Cross section of minor helical-wrinkled tube (view of axial-radial plane).	4
3.	Cross section of hoop-wrinkled tube (view of radial-circumferential plane).....	4
4.	Cross section of severe helical-wrinkled tube (view of axial-radial plane).....	4
5.	Impact load versus impact energy with and without incompressible polymeric insert.....	5
6.	Photographs showing the impact damage from an impact load of 136.4 kg (300 lb) (with an incompressible polymeric insert).....	6

7. Burst pressure versus impact load.	6
8. Longitudinal failure mode and subtracted images showing the failure sequence of specimen with no fabricated wrinkle (at 13500 frames/s).	7
9. Slanted failure mode and subtracted images showing the failure sequence of specimen with no fabricated wrinkle (at 13500 frames/s).	7
10. Failure mode and subtracted images showing the failure sequence of specimen with a hoop wrinkle (at 13500 frames/s).....	8
11. Failure mode and subtracted images showing the failure sequence of specimen IV-1 (at 13500 fps).....	9
12. Failure mode and subtracted images showing the failure sequence of specimen IV-2 (at 13500 fps).....	9
13. Failure mode and subtracted images showing the failure sequence of specimen IV-5 (at 13500 frames/s).....	10

1. Introduction

Two test series were conducted to assess the strength degradation of filament-wound graphite/epoxy (Gr/Ep) tubes caused by either impact damage or fabrication defects. The tubes were fabricated from Toho G30-500-12K PAN fibers in Epon 828 epoxy resin.¹ They typically had a lay-up pattern of $(+10^\circ, -10^\circ, 90^\circ)_3$, (six 10° helical layers and three hoop layers). The inner diameter of the tubes was 10.2 cm (4 in.), and the wall thickness was a nominal 1.83 mm (0.072 in.). The tubes were wound in 335.3-cm (11-ft) lengths and cut into 38.1-cm (15-in.) lengths for testing. The composite tubes were subjected to internal pressure, thereby creating a biaxial stress-state in the tube walls with a hoop stress equal to twice the axial stress. End-fittings were designed for sealing the ends of the tubes without slipping.² Internal rubber bladders were used to prevent leaking so that the pressure could be maintained at a constant level. The assembled specimen with its end fittings is depicted in Figure 1. Each experiment was filmed with a Kodak high-speed video camera operating at 9000 to 13,500 frames/s to determine the location of fracture initiation and to observe the burst dynamics.

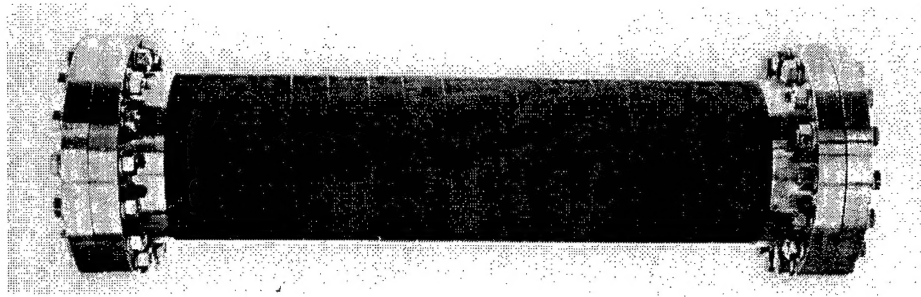


Figure 1. Outside view of tube specimen with end fittings.

2. Test Series

2.1 Tubes with Impact Damage

The impact damage was made by a pendulum-type impactor. The impactor consisted of a steel frame, a 1.6-mm (0.062-in.) diameter steel cable, and an impacting mass of cylindrical shape. The swing arc radius was 1.6 m (64 in.). Two different brass impact masses, 2.53 and 4.43 kg (5.57 lb and 9.75 lb), were used. A 6.3 mm (0.25 in.) diameter steel tup was inserted into the tip of each impacting mass. The impact was conducted by placing the specimen with its axis oriented horizontally in a V-groove made from aluminum. The V-groove and the specimen were then fastened to a heavy steel frame so that the specimen would not move during impact. The specimen was placed such that the impact pendulum would be moving horizontally at the point of impact and such that the impact velocity would be normal to the surface of the specimen. The impact damage was conducted with either an empty tube, or with a piece of nearly incompressible polymeric material snugly fitted inside the specimen. The latter case represented a much stiffer condition and, at constant impact energy, gave a much higher impact load. During the impact operation, the initial and rebound impactor locations were measured, allowing the calculation of impact energy and the energy absorbed.

The tubes were subjected to either hydraulic or pneumatic pressure. For the pneumatic-tested specimens, there was either a plastic insert that had an outside diameter about 6.3 mm (0.25 in.) less than the inner diameter (ID) of the tube, or an insert made of nearly incompressible material. The latter insert fitted snugly into the ID of the tube and had a 1.27-cm (0.5-in.) diameter bore through which the pressure was applied to the tube until bursting.

2.2 Tubes with Fabricated Defects

Graphite-epoxy tubes of lay-up ($+10^\circ$, -10° , 90°) were procured with different wrinkle conditions (1) no wrinkles, (2) a minor wrinkle in one helical layer, (3) a wrinkle in one hoop layer, and (4) a major helical wrinkle. The last group of tubes had a lay-up of ($+15^\circ$, -15° , 90° , 90°)₃. The purpose of this lay-up was to induce helical fiber-dominated failures. All as-received tubes underwent ultrasonic inspection to ensure that no delaminations or other unintended flaws were present before testing. The cross sections of helical and hoop wrinkles in tubes two, three, and four are shown in Figures 2 through 4, respectively.

The helical wrinkles were created using circular resin rings cured in advance. The rings were circumferentially placed at designated locations 38.1 cm (15 in.) apart during the winding operation. The minor helical wrinkles were caused by placing a single ring below the middle helical layer. The more severe helical wrinkles were caused by placing one ring below the middle helical layer and two rings above this layer to ensure maximum curvature of the wrinkle. The hoop wrinkles were created using two 20.3-cm (8-in.) long graphite/epoxy rods fully cured in advance. The two rods ran longitudinally through each segment. One rod was below and the other was above the second hoop layer.

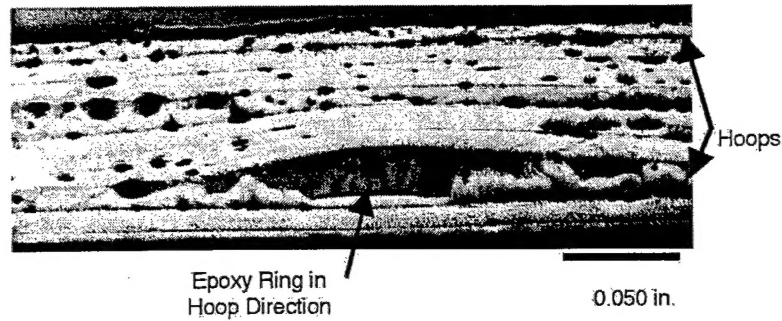


Figure 2. Cross section of minor helical-wrinkled tube (view of axial-radial plane).

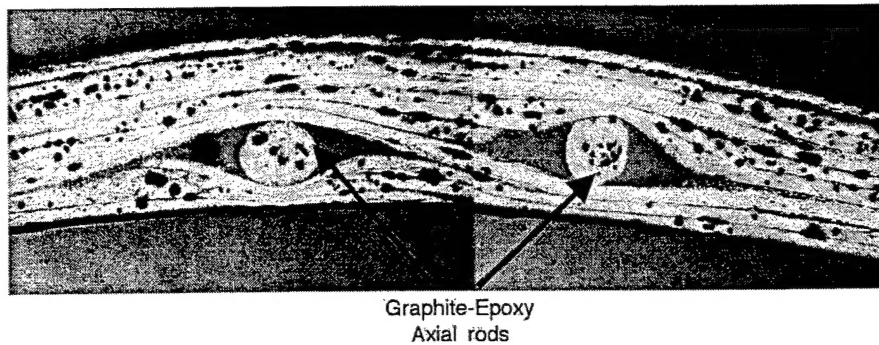


Figure 3. Cross section of hoop-wrinkled tube (view of radial-circumferential plane).



Figure 4. Cross section of severe helical-wrinkled tube (view of axial-radial plane).

The wrinkled tube sections were tested under two conditions: either pressurized directly to burst, or proof tested before burst. For each proof cycle, the pre-determined proof pressure was applied with the peak pressure maintained for 2 min before venting. As many as six proof-test cycles were performed on a single tube to see whether the manufactured defect might propagate and further weaken the tube. Proof pressures up to ~95% of burst and number of proof testing cycles had no noticeable effect on the average ultimate burst pressures of the tubes. With only one exception, all of the tubes burst at a higher pressure than the proof pressures applied. The lone sample that failed at a lower pressure was proofed three times to 98% of the average burst pressure and failed at a pressure about 0.2% lower than the pressure applied for the three prior proof cycles.

3. Test Results

3.1 Tubes with Impact Damage

Figure 5 depicts the impact load vs. impact energy plot using two different masses, 2.53 and 4.43 kg (5.57 and 9.75 lb). It shows that a tube filled with nearly incompressible polymeric material experiences an impact load as much as 50% more than that for an unfilled tube for the same incident energy.

The impact loads typically produced damage consisting of one or two visible line cracks. Photographs of a typical crack are shown in Figure 6. The cracks ran either in the longitudinal or in an off-axis direction. They were typically 1.3 to 1.9-cm (0.5 to 0.75-in.) long depending on the magnitude of the impact. Figure 7 shows the burst pressure as a function of impact load. It shows that the burst pressure decreases significantly with increasing impact force. For impact loads of 823 to 1470 newtons (N) (185 to 330 lb), the burst pressure dropped by as much as 24% to 32%, respectively, compared to the burst pressure of tubes with no impact damage.

Most failures initiated at the impact locations. However, from the high-speed camera images, it was apparent that the failures of the impact-damaged tubes did not necessarily originate at the impact sites. Of the 14 impact-damaged tubes, four burst with failure initiation points away from the impact location. This suggests that different types of damage can occur in tubes that receive essentially identical impacts. It is speculated that the failure initiation away from the impact location may be the result of impact-induced bending stress. An impact to the tube will create a stress wave propagating in both longitudinal and circumferential directions. The wave-induced deformation will subsequently generate bending moments throughout the entire tube at various times. The bending stress can be high because of the thin wall thickness of the tube, and the compressive stress may cause fiber buckling if a local defect exists. When fibers buckle, they lose their load-carrying ability, and the buckled region becomes the weakest link. Failure will then initiate from this region during subsequent pressure loading. For a more detailed description and discussion, see Refs. 3 and 4.

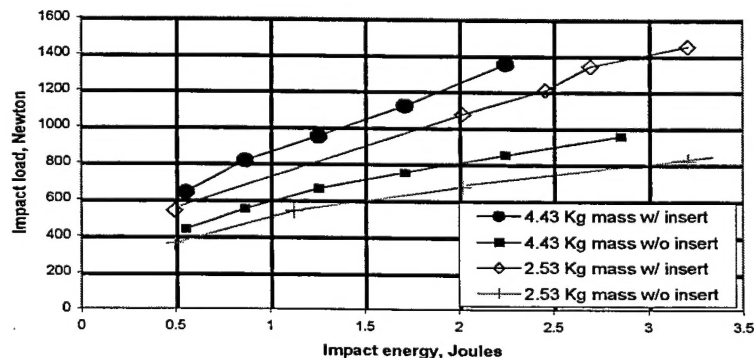


Figure 5. Impact load versus impact energy with and without incompressible polymeric insert (two impact masses).

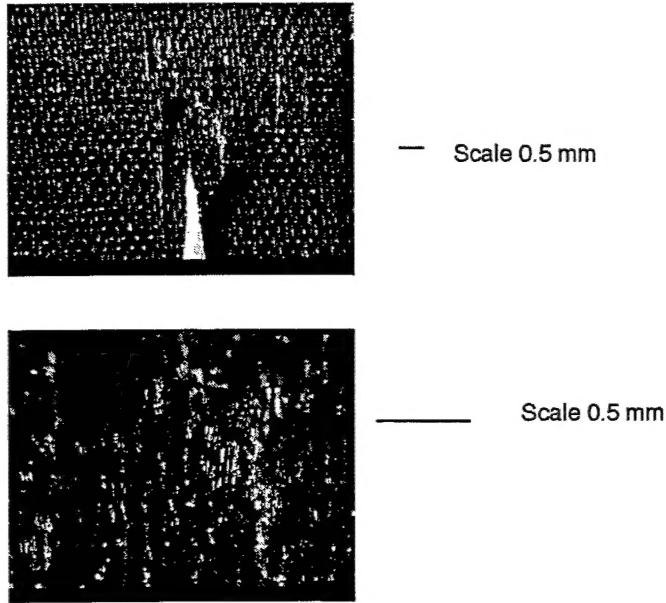


Figure 6. Photographs showing the impact damage from an impact load of 136.4 kg (300 lb) (with an incompressible polymeric insert).

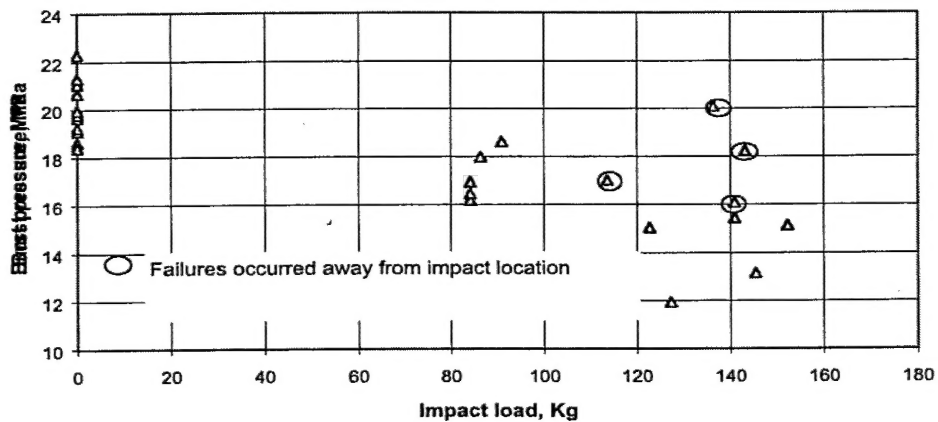


Figure 7. Burst pressure versus impact load.

3.2 Tubes with Fabricated Defects

3.2.1 Tubes Without Wrinkles

A total of nine specimens were fabricated and tested for this group. The tube specimens were typically 38.1 cm (15 in.) long. The average burst pressure was 19.7 MPa (2860 psi). There are typically two fracture modes for this series. One was a longitudinal mode with a crack running primarily in the axial direction. The second type of failure mode was a slanted crack at about 45° from the axial direction. Figures 8 and 9 depict the two types of failures as well as the subtracted frames from their respective reference frame at 74- μ s time intervals. In Figures 8 and 9, there are two tube images in

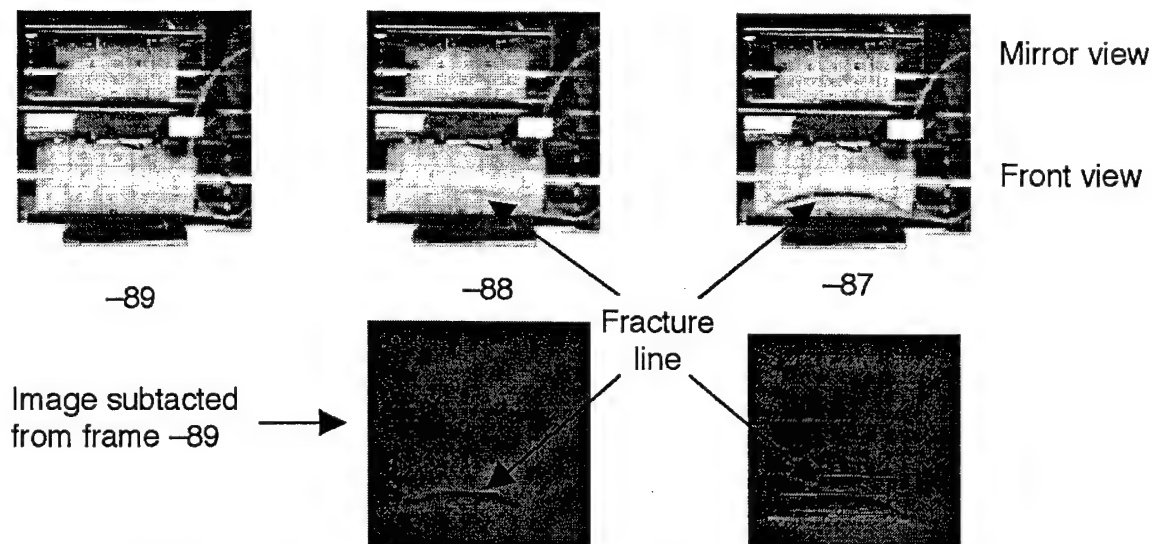


Figure 8. Longitudinal failure mode and subtracted images showing the failure sequence of specimen with no fabricated wrinkle (at 13500 frames/s).

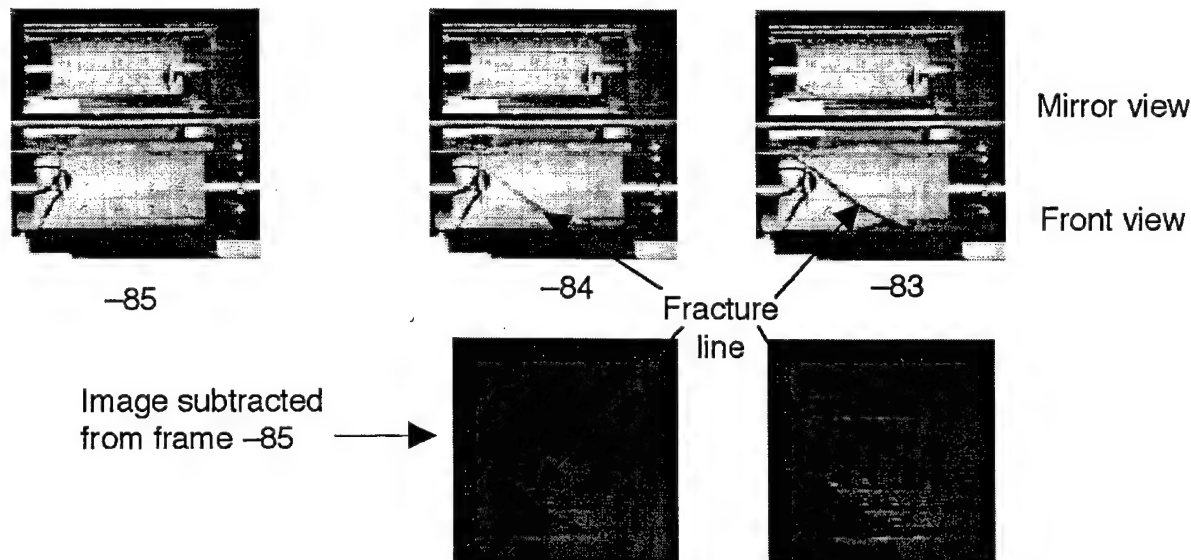


Figure 9. Slanted failure mode and subtracted images showing the failure sequence of specimen with no fabricated wrinkle (at 13500 frames/s).

each frame because a mirror was installed to reflect the image of the back surface of the specimen so that the fracture initiation would be captured if the fracture initiated from the back surface.

3.2.2 Tubes With Minor Helical Defects

The average burst pressure for the wrinkled tubes was 20.8 MPa (3022 psi). The helical wrinkle did not noticeably degrade the tube strength. One reason is that the strength of the tube is dominated by the hoop fibers. The composite stress in the hoop direction is twice the stress in the axial direction. However, the number of helical fibers is twice that of the hoop fibers. This results in an approximate

factor of 4 in the fiber-to-stress ratio in the helical direction as compared to the hoop direction. (The reduction of the strength due to a 10° inclination of the helical fibers from the axial direction is small.) Although there was some strength degradation to the helical fibers from the helical wrinkles, the degradation was not enough to cause any helically dominated failures. The failure modes of this series are similar to those observed in the non-wrinkled specimens: either a longitudinal fracture mode or an inclined fracture mode.

3.2.3 Tubes With Hoop Defects

Hoop wrinkles significantly reduce the burst pressure. The fabricated hoop wrinkle was much more effective in degrading the strength than the helical wrinkle. The burst pressures range from 15.1 to 18.7 MPa (2195 to 2716 psi). The strength reduction averaged 14% and was as much as 23% of the pressure for un-wrinkled specimens. Figure 10 depicts a failure as well as the subtracted frames from the respective reference frame at 74- μ s time intervals. The fractures are all longitudinal.

3.2.4 Tubes With Severe Helical Defects

A total of three wrinkled and two non-wrinkled specimen from this $(+15^\circ, -15^\circ, 90^\circ, 90^\circ)_3$ tube were tested. The average burst pressure of non-wrinkled specimens was 52.82 MPa (7658 psi), and the average burst pressure for wrinkled tubes was 48.82 MPa (7078 psi). This gives a 7.6% average strength reduction. The failure mode of the specimens in this test series is different from those in the previous three groups in which the failures were dominated by the hoop fibers with little influence from the helical fibers. This was true because there were half as many fibers in the hoop direction as

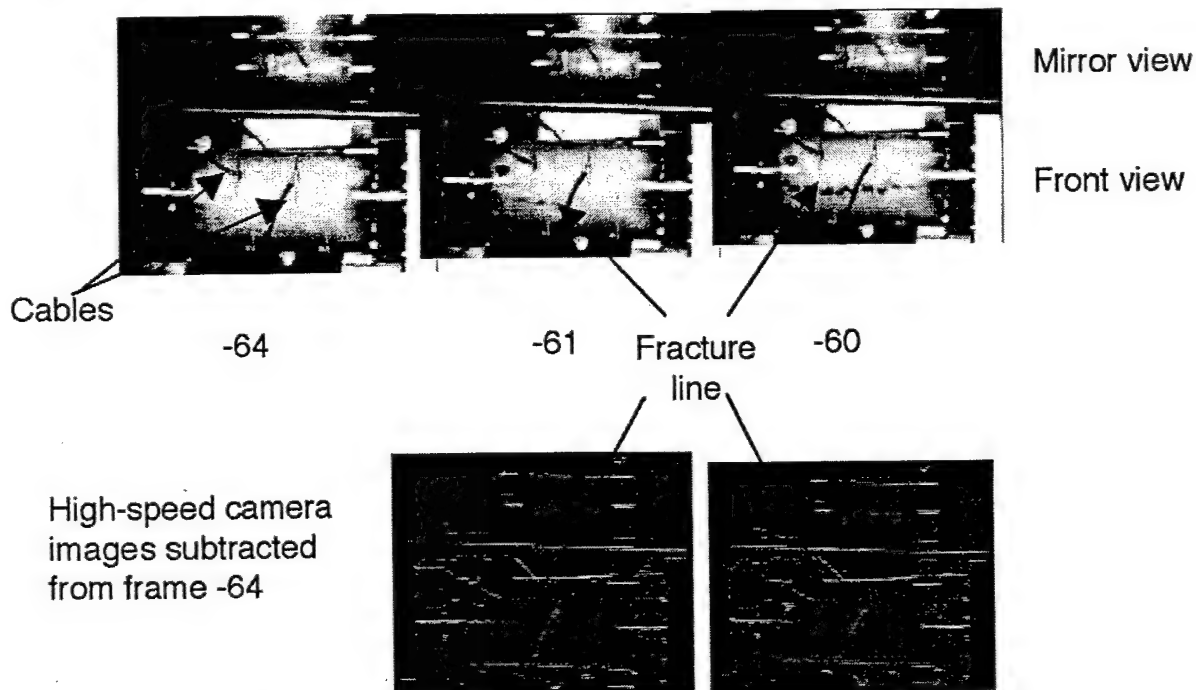


Figure 10. Failure mode and subtracted images showing the failure sequence of specimen with a hoop wrinkle (at 13500 frames/s).

in the helical direction, while the hoop stress was twice the stress in the axial direction. For this series, the number of fibers is more or less balanced in both directions. The stress in the helical fibers became more significant at burst pressure, especially in the wrinkle region. Figures 11 through 13 depict the subtracted images for specimens IV-1, IV-2, and IV-5. Specimen IV-1 had no wrinkle, while specimens IV-2 and IV-5 were wrinkled. From these three figures, it can be seen that the failure for specimen IV-1 was hoop-fiber dominated, the failure of specimen IV-2 was mixed, and the failure of specimen IV-5 was helical-fiber dominated.

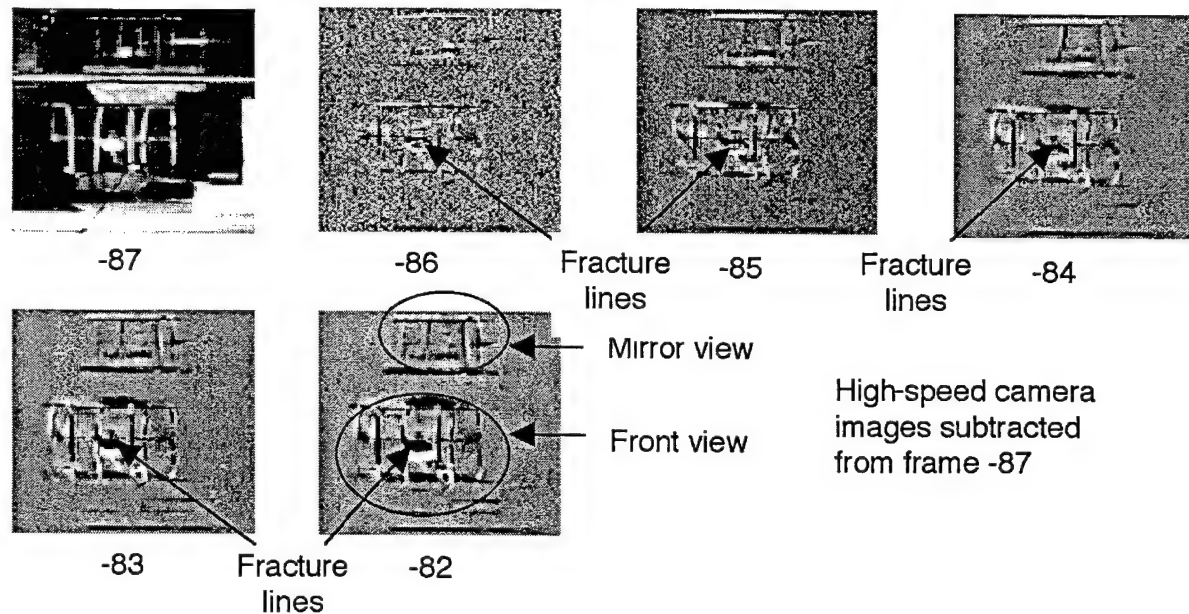


Figure 11. Failure mode and subtracted images showing the failure sequence of specimen IV-1 (at 13500 fps).

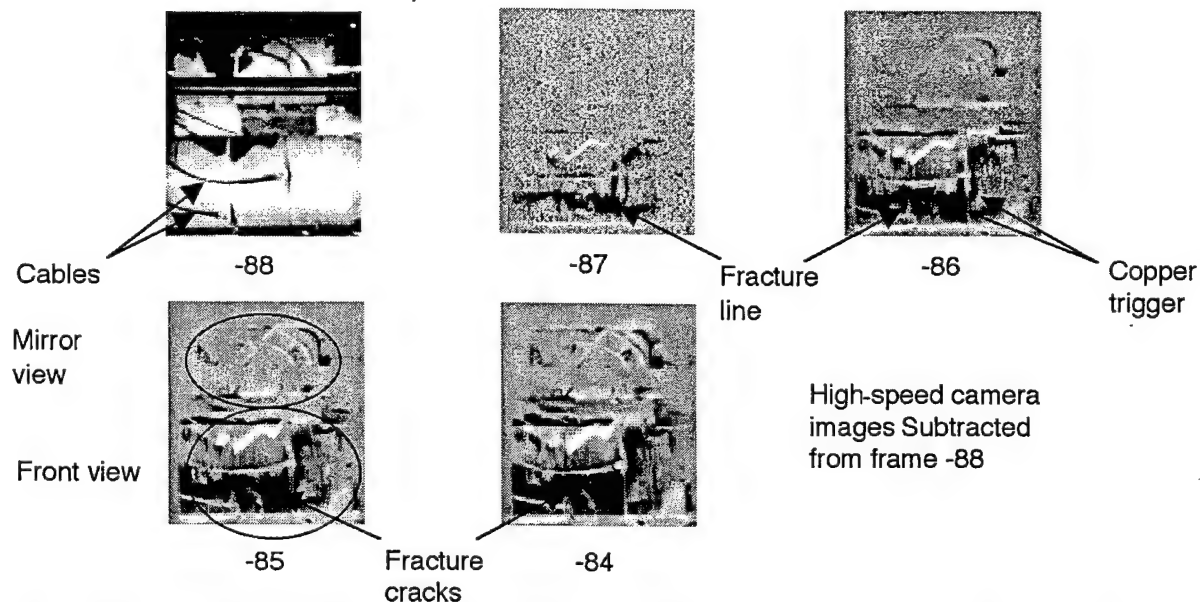


Figure 12. Failure mode and subtracted images showing the failure sequence of specimen IV-2 (at 13500 fps).

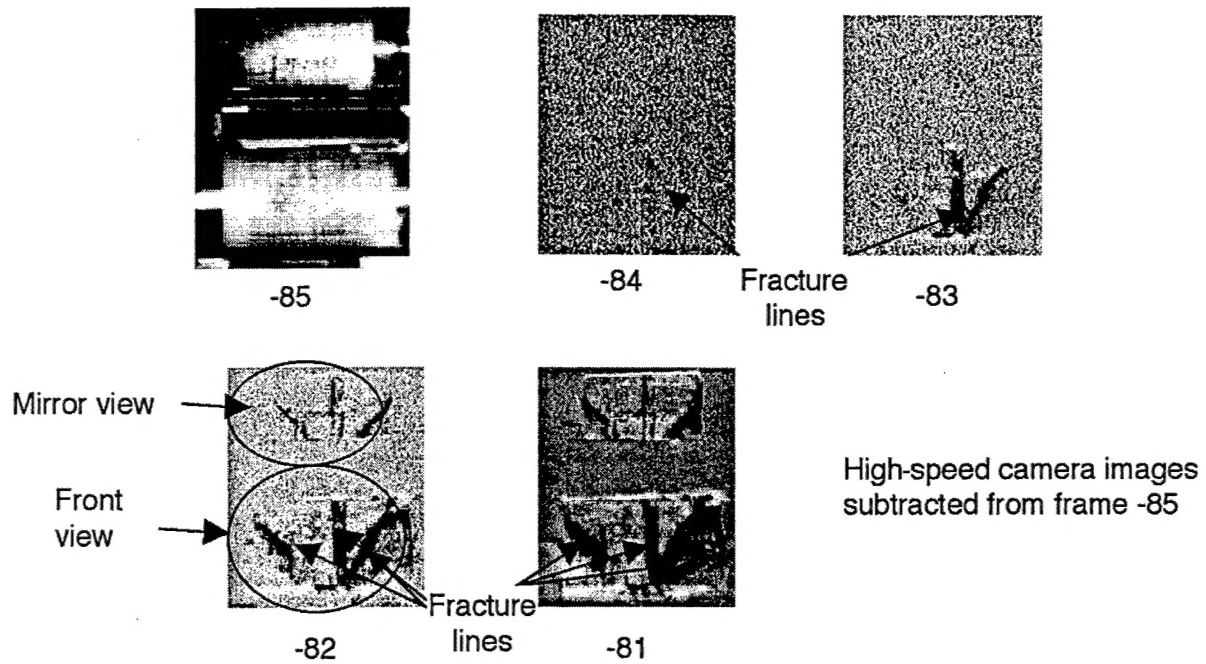


Figure 13. Failure mode and subtracted images showing the failure sequence of specimen IV-5 (at 13500 frames/s).

4. Summary

Two test series were conducted to assess the strength degradation of filament-wound graphite/epoxy (Gr/Ep) tubes caused by either impact damage or fabrication defects. The tubes were fabricated from Toho G30-500-12K PAN fibers in Epon 828 epoxy resin. The baseline tube configuration had a nine-ply $(+10^\circ, -10^\circ, 90^\circ)_3$ lay-up. This lay-up configuration was for all the impact-and wrinkle-defected specimens with the exception of one tube that had a $(+15^\circ, -15^\circ, 90^\circ, 90^\circ)_3$ stacking sequence. The latter lay-up configuration, which also had fabricated helical defects, was to induce helical fiber-dominated failure.

The test results on impact-damaged specimens show that the burst pressure decreases significantly with increasing impact force. For impact loads of 823 to 1470 N (185 to 330 lb), the burst pressure dropped by as much as 24% to 32%, respectively, compared to the burst pressure of tubes with no impact damage. The failures initiated primarily from the impact locations. However, some of the failures did not originate at the impact sites. This suggests that different types of damage can occur in tubes that receive essentially identical impacts.

The test results for wrinkled tubes lead to the following observations:

- The minor helical wrinkles did not measurably affect the burst pressure. The more severe helical wrinkles caused an average reduction in burst pressure of 8%. Hoop wrinkles caused a significant degradation in strength (14% on average).
- Failure initiations and propagations were documented with a high-speed camera. In the tubes with wrinkles, the failures initiated in the immediate vicinity of the wrinkles. There were two failure modes for un-wrinkled tubes and tubes with minor helical wrinkles: a longitudinal mode and an inclined mode. The failure mode for all of the tubes with hoop wrinkles was longitudinal. The failure modes of severe helical-wrinkled tubes were multiple typed. Since the fiber stresses in the helical fibers are more balanced with those in the hoop fibers, the failures were significantly affected by the wrinkles. The failure modes varied from hoop fiber-dominated for un-wrinkled tubes to mixed and helical-fiber dominated for wrinkled tubes.
- Proof pressures up to ~95% of burst and number of proof testing cycles had no noticeable effect on the average ultimate burst pressures of the tubes. With only one exception, all of the tubes burst at a higher pressure than the proof pressures applied. The lone sample that failed at a lower pressure was proofed three times to 98% of the average burst pressure and failed at a pressure about 0.2% lower than the pressure applied for the three prior proof cycles.
- The tubes were not NDE inspected. For discussion of NDE work on the tubes with fabrication defects, readers are referred to Ref. 5.

References

1. Made by Advanced Composite and Products Technology, Huntington Beach, CA.
2. U.S. Pat. 6,253,599, Pressure Vessel Testing Fixture (July 3, 2001) D. J. Chang and P. R. Valenzuela.
3. D. J. Chang, P. R. Valenzuela, and T. V. Albright, "Burst Tests of Filament-wound Graphite-epoxy Tubes—Pathfinder Test Series For Delta II GEM Motor Cases," Aerospace Report No. TR-2000(1494)-1, The Aerospace Corporation, 20 Dec 2000.
4. D. J. Chang, "Burst Tests of Filament-Wound Graphite-Epoxy Tubes," *Journal of Composite Materials*, Vol. 37, No. 9, May 2003.
5. D. J. Chang, et al, "Burst Testing of Filament-Wound Graphite-Epoxy Composite Tubes," Aerospace Report No. TR-2001(1413)-3, The Aerospace Corporation, 1 November 2002.

LABORATORY OPERATIONS

The Aerospace Corporation functions as an "architect-engineer" for national security programs, specializing in advanced military space systems. The Corporation's Laboratory Operations supports the effective and timely development and operation of national security systems through scientific research and the application of advanced technology. Vital to the success of the Corporation is the technical staff's wide-ranging expertise and its ability to stay abreast of new technological developments and program support issues associated with rapidly evolving space systems. Contributing capabilities are provided by these individual organizations:

Electronics and Photonics Laboratory: Microelectronics, VLSI reliability, failure analysis, solid-state device physics, compound semiconductors, radiation effects, infrared and CCD detector devices, data storage and display technologies; lasers and electro-optics, solid-state laser design, micro-optics, optical communications, and fiber-optic sensors; atomic frequency standards, applied laser spectroscopy, laser chemistry, atmospheric propagation and beam control, LIDAR/LADAR remote sensing; solar cell and array testing and evaluation, battery electrochemistry, battery testing and evaluation.

Space Materials Laboratory: Evaluation and characterizations of new materials and processing techniques: metals, alloys, ceramics, polymers, thin films, and composites; development of advanced deposition processes; nondestructive evaluation, component failure analysis and reliability; structural mechanics, fracture mechanics, and stress corrosion; analysis and evaluation of materials at cryogenic and elevated temperatures; launch vehicle fluid mechanics, heat transfer and flight dynamics; aerothermodynamics; chemical and electric propulsion; environmental chemistry; combustion processes; space environment effects on materials, hardening and vulnerability assessment; contamination, thermal and structural control; lubrication and surface phenomena. Microelectromechanical systems (MEMS) for space applications; laser micromachining; laser-surface physical and chemical interactions; micropropulsion; micro- and nanosatellite mission analysis; intelligent microinstruments for monitoring space and launch system environments.

Space Science Applications Laboratory: Magnetospheric, auroral and cosmic-ray physics, wave-particle interactions, magnetospheric plasma waves; atmospheric and ionospheric physics, density and composition of the upper atmosphere, remote sensing using atmospheric radiation; solar physics, infrared astronomy, infrared signature analysis; infrared surveillance, imaging and remote sensing; multispectral and hyperspectral sensor development; data analysis and algorithm development; applications of multispectral and hyperspectral imagery to defense, civil space, commercial, and environmental missions; effects of solar activity, magnetic storms and nuclear explosions on the Earth's atmosphere, ionosphere and magnetosphere; effects of electromagnetic and particulate radiations on space systems; space instrumentation, design, fabrication and test; environmental chemistry, trace detection; atmospheric chemical reactions, atmospheric optics, light scattering, state-specific chemical reactions, and radiative signatures of missile plumes.